ADVANCED FUNCTIONAL MATERIALS
www.afm-journal.de

Molecular-Scale Strategies to Achieve High Efficiency and Low Efficiency Roll-off in Simplified Solution-Processed Organic Light-Emitting Diodes

Young-Hoon Kim, Tae-Hee Han, Changsoo Lee, Yun-Hi Kim, Yang Yang, and Tae-Woo Lee**

Solution-processed small-molecule organic light-emitting diodes (OLEDs) are regarded as next-generation flat-panel displays and solid-state lighting sources due to low material loss and a simple device fabrication process. However, they still suffer from low device efficiency and severe efficiency roll-off. Here, molecular-scale strategies are proposed to achieve highly efficient solution-processed small-molecule OLEDs with reduced efficiency roll-off. By combining experiments with ab initio and molecular dynamics simulations, it is shown that an acetylacetonate group in a phosphorescent dopants lowers the dipole moment and molecular interaction energy of dopants, reducing dopant aggregation and increasing charge carrier transport. Furthermore, a charge-balance assistant molecule is incorporated in the mixed-host emitting layer to increase the balance of charge carrier transport and to broaden the exciton recombination zone in the center of the emitting layer. The resulting OLEDs have a current efficiency (CE) of 103.7 cd A^{-1}, which is the highest yet reported in solution-processed OLEDs, and low efficiency roll-off (CE = 99.68 cd A^{-1} at a luminance L_{EL} = 100 cd m^{-2}, and CE = 75.00 cd A^{-1} at L_{EL} = 1000 cd m^{-2}) even with the simplified device architecture. It is expected that this strategy will advance the feasibility of commercialization of low-cost high-efficiency OLEDs.

1. Introduction

Organic light-emitting diodes (OLEDs) have various advantages such as light weight, flexibility, compatibility with mass production, and high electroluminescence (EL) efficiency.[1–5] However, most of efficient OLEDs have had multilayered structure and been fabricated by vacuum thermal deposition, which is expensive, complex, and incompatible with roll-to-roll printing.[6–11] Minimizing the manufacturing cost of OLEDs is a major challenge for mass production and commercialization of large-size displays and solid-state lighting.[12–14] Therefore, low-cost solution-processed OLEDs that have simple structure and high EL efficiency must be developed further.

Recently, high EL efficiencies in solution-processed OLEDs have been obtained by using diphenylbis(3-(pyridine-2-yl) phenyl)silane (2PTPS) as an electron transport host in an emitting layer.[15] 2PTPS has high electron mobility ($\approx 3 \times 10^{-4}$ cm^2 V^{-1} s^{-1}) and induces direct charge trapping in the phosphorescent dopants, facilitating balanced charge transport and efficient exciton recombination in the emitting layer. Use of this strategy achieved high current efficiency CE = 101.5 cd A^{-1} in solution-processed OLEDs based on green-emitting phosphorescent dopants (tris[2-phenylpyridinato-C2,N]iridium(III) ($Ir(ppy)_3$)).[15] However, the solution-processed OLEDs still undergo severe efficiency roll-off which is a reduction in EL efficiency as luminance increases. Efficiency roll-off reduces the actual efficiency of devices in practical brightness levels of applications such as mobile

Dr. Y.-H. Kim, Dr. T.-H. Han, Prof. T.-W. Lee
Department of Materials Science and Engineering
Institute of Engineering Research
Research Institute of Advanced Materials
Nano Systems Institute (NSI)
BK21 PLUS SNU Materials Division for Educating Creative Global Leaders
Seoul National University
1 Gwanak-ro, Gwanak-gu, Seoul 08826, Republic of Korea
E-mail: taewlees@gmail.com; twlees@snu.ac.kr

Dr. T.-H. Han
Division of Materials Science and Engineering
Hanyang University
Seoul 04763, Republic of Korea
E-mail: taeheehan@hanyang.ac.kr

The ORCID identification number(s) for the author(s) of this article can be found under https://doi.org/10.1002/adfm.202005292.

Dr. T.-H. Han, Dr. C. Lee, Prof. Y. Yang
Department of Materials Science and Engineering
University of California
Los Angeles, CA 90095, USA

Dr. C. Lee
Department of Materials Science and Engineering
Korea Advanced Institute of Science and Technology
291 Daehak-ro, Yuseong-gu, Daejeon 34141, Republic of Korea

Prof. Y.-H. Kim
Department of Chemistry and Research Institute of Natural Science
Gyeongsang National University
Jinju-daero, Jinju-si, Gyeongsangnam-do 501, Republic of Korea

Prof. T.-W. Lee
School of Chemical and Biological Engineering
Seoul National University
1 Gwanak-ro, Gwanak-gu, Seoul 08826, Republic of Korea

DOI: 10.1002/adfm.202005292

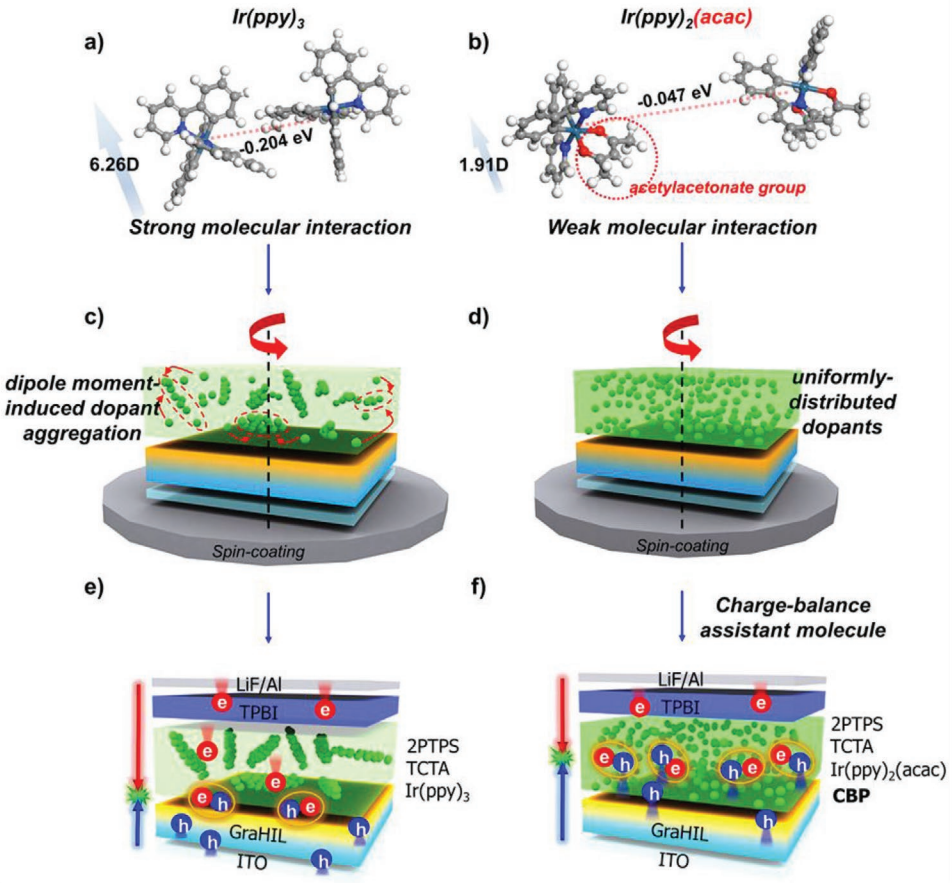

Figure 1. Dipole moment and molecular interaction energy of a) $Ir(ppy)_3$ and b) $Ir(ppy)_2(acac)$ calculated by density functional theory (DFT) simulation (gray dot: carbon, white dot: hydrogen, blue dot: iridium (Ir), red dot: oxygen). Molecular distribution of c) $Ir(ppy)_3$ and d) $Ir(ppy)_2(acac)$ during spincoating of emitting layer. Operating mechanism of solution-processed OLEDs based on e) high-*m* (2PTPS:TCTA:$Ir(ppy)_3$) and f) CBP:low-*m* (2PTPS:TCTA:$Ir(ppy)_2(acac)$) films.

displays (100–400 cd m^{-2}), television displays (<1000 cd m^{-2}), indoor lighting (<5000 cd m^{-2}) and large-area lighting (>5000 cd m^{-2}),[16,17] and leads to high power consumption and excessive heat generation of devices. Therefore, to fulfill industrial standards and extend the range of applications such as traffic lighting, daylight displays or lighting, the efficiency roll-off of solution-processed OLEDs should be reduced.

The efficiency roll-off in phosphorescent OLEDs basically arises from 1) triplet–triplet annihilation (TTA) and triplet–polaron annihilation (TPA) due to the long lifetime of excited phosphorescent states (approximately microseconds to milliseconds),[16,18,19] and 2) charge imbalance[20,21] and electric-field-induced exciton loss (i.e., exciton dissociation by applied electric field).[22,23] In solution-processed phosphorescent OLEDs, small organic molecules have low solubility in organic solvents and easily aggregate in the emitting layer, so the efficiency roll-off could be even worse than that in vacuum-deposited counterparts.[7,24,25] The molecular aggregates increase the severity of TTA and TPA between dopant molecules because triplet excitons are populated and annihilated.[16,18,19] Solution processing cannot easily fabricate multilayered device structure due to intermixing between layers,[26] inducing charge imbalance.[16] Therefore, dopant aggregation and charge imbalance in the emitting layer should be prevented to reduce efficiency roll-off in solution-processed phosphorescent OLEDs.

Here, we demonstrated highly efficient solution-processed phosphorescent OLEDs with low efficiency roll-off by combining two molecular-scale strategies (**Figure 1**). First, we employed phosphorescent dopant in which one acetylacetonate group is attached to the central Iridium. By combining experiments with ab initio and molecular dynamics simulations, we showed that acetylacetonate group reduces dipole moment and molecular interaction energy of dopants, preventing aggregation-induced exciton quenching and increasing charge-carrier transport. We also incorporated charge-balance assistant molecule in the mixed-host emitting layer to increase balanced charge carrier transport and broaden exciton recombination zone in the center of the emitting layer by facilitating hole transport and suppressing electron transport. With these comprehensive strategies, we achieved CE = 103.7 cd A^{-1}, which is to our best knowledge the highest yet reported in solution-processed OLEDs, and low efficiency roll-off (CE of 99.68 cd A^{-1} at a luminance L_{EL} = 100 cd m^{-2}, 75.00 cd A^{-1} at L_{EL} = 1000 cd m^{-2}) even with simple device structure.

2. Results and Discussion

First, we conducted density functional theory (DFT) simulation to study the effects of acetylacetonate group on phosphorescent dopants (Figure 1a,b, top). We compared $Ir(ppy)_3$ with bis(2-phenylpyridine) (acetylacetonate) iridium(III) ($Ir(ppy)_2(acac)$) in which one acetylacetonate group is attached to the central Iridium. DFT results indicate that acetylacetonate group reduces the dipole moment m of phosphorescent dopant therefore, $Ir(ppy)_2(acac)$ has lower m (1.91 D) and molecular interaction energy (–4.512 kJ mol^{-1}; –0.047 eV) than does $Ir(ppy)_3$ (m = 6.26 D and molecular interaction energy = –19.584 kJ mol^{-1}; –0.204 eV). Here, a negative value means greater interaction energy between dopant molecules. Reduced m and molecular interaction energy can increase dopant distribution in molecular-scale and decrease interaction between dopants and charge carriers,[27–29] facilitating charge transport.

To study the effects of reduced m and molecular interaction energy by acetylacetonate group on dopant distributions in emitting layer, we simulated distributions of dopants ($Ir(ppy)_3$ or $Ir(ppy)_2(acac)$), tris(4-carbazoyl-9-ylphenyl)amine (TCTA) and 2PTPS in tetrahydrofuran (THF) solvent by molecular dynamics (MD). The number of each dopant, TCTA and 2PTPS was set to be 50. MD simulation reveals that $Ir(ppy)_3$ molecules are more aggregated in TCTA:2PTPS:THF than $Ir(ppy)_2(acac)$ molecules (**Figure 2**a–d). Simulated radial distribution function (RDF) shows

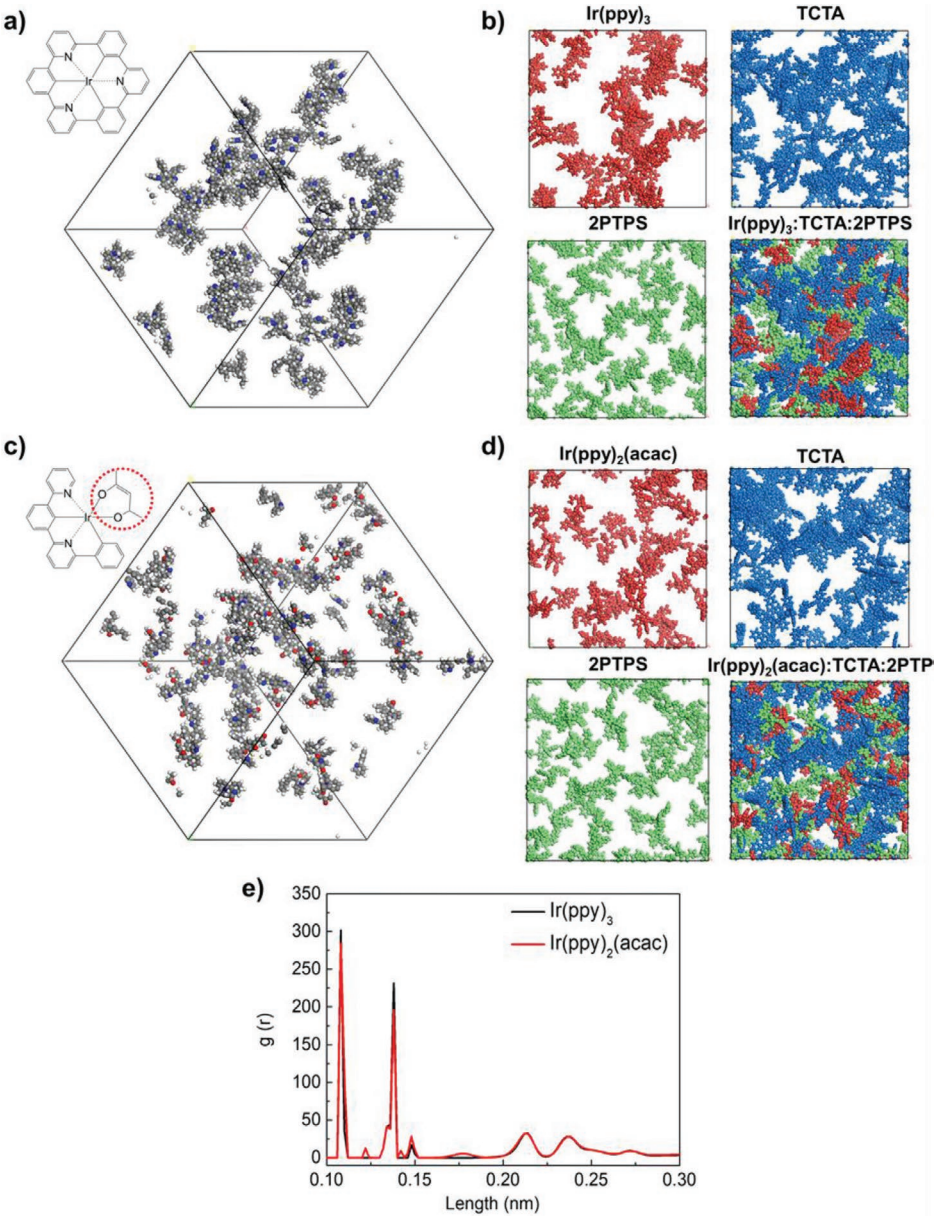

Figure 2. a) 3D molecular distributions of $Ir(ppy)_3$, b) 2D molecular distributions of $Ir(ppy)_3$, TCTA and 2PTPS, c) 3D molecular distributions of $Ir(ppy)_2(acac)$, d) 2D molecular distributions of $Ir(ppy)_2(acac)$, TCTA and 2PTPS. e) Calculated radial distribution function (RDF) of $Ir(ppy)_3$ and $Ir(ppy)_2(acac)$ in TCTA:2PTPS:THF system. Data were calculated by molecular dynamics (MD) simulation.

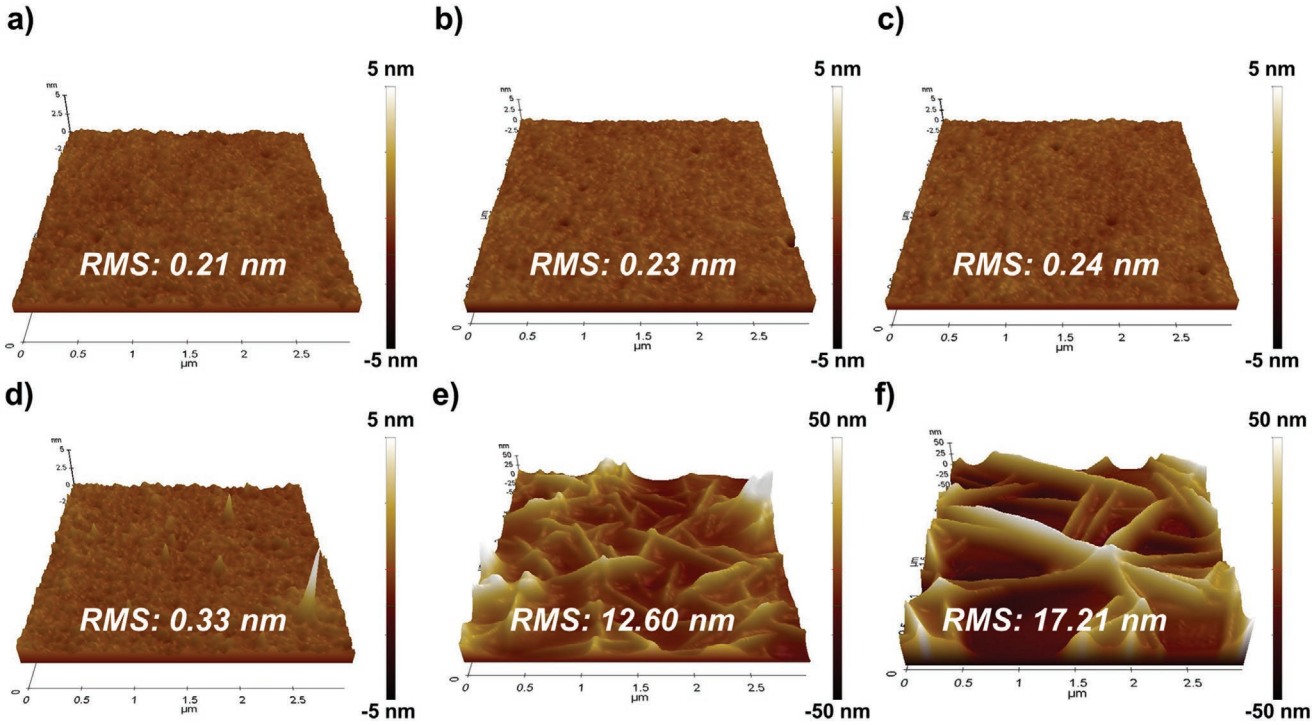

Figure 3. Atomic force microscope (AFM) images of solution-processed low-*m* ($Ir(ppy)_2(acac)$:TCTA:2PTPS) films with different dopant concentration: a) 15 wt%, b) 30 wt%, c) 60 wt%, and high-*m* ($Ir(ppy)_3$:TCTA:2PTPS) films with different dopant concentration: d) 15 wt%, e) 30 wt%, f) 60 wt%. Thicknesses of all films are fixed to 40 nm.

that $Ir(ppy)_3$ has higher molecular density than does $Ir(ppy)_2(acac)$ in a close molecular distance (<0.15 nm) (Figure 2e), confirming that $Ir(ppy)_3$ molecules are more aggregated in TCTA:2PTPS host molecules than $Ir(ppy)_2(acac)$ molecules.

To study the effects of dopant distribution on film morphology, we fabricate TCTA:2PTPS:$Ir(ppy)_2(acac)$ (low-*m*) and TCTA:2PTPS:$Ir(ppy)_3$ (high-*m*) films with different dopant concentrations [*D*]. Low-*m* films with [*D*] ≈15 wt% had low root mean-squared roughness r_{rms} = 0.21 nm with uniform film morphology, whereas high-*m* films with [*D*] ≈15 wt% had r_{rms} = 0.33 nm with some spiking regions (height > 5 nm) (**Figure 3**). We attribute this to the fact that $Ir(ppy)_2(acac)$ has higher solubility (>0.1 wt%) in THF than does $Ir(ppy)_3$ (<0.03 wt%) because $Ir(ppy)_2(acac)$ has similar *m* (≈1.91 D) with THF (*m* ≈ 1.63 D) than does $Ir(ppy)_3$ (*m* ≈ 6.26 D).[27,28] As [*D*] increases to 60 wt%, low-*m* films showed uniform film morphology with constant r_{rms} (0.21–0.24 nm), however, high-*m* films showed needle-shaped aggregates (>3 µm in length) with significantly increased r_{rms} (17.21 nm). Formation of needle-like aggregates of $Ir(ppy)_3$ molecules could be due to 1) polarity difference and immiscibility between $Ir(ppy)_3$ and host molecules[30] and 2) intermolecular interaction[31] or self-assembly[32,33] into 1D microstructures as a result of high *m* of $Ir(ppy)_3$.[27,28]

As [*D*] increased, low-*m* films showed less decreases in steady-state photoluminescence (PL) intensity L_{PL} and in relative PL intensities under the continuous excitation, $L_{PL,rel}$ = (L_{PL} of film with [*D*] = *x* wt%)/(L_{PL} of film with [*D*] = 1 wt%), than did high-*m* counterparts (**Figure 4**a–d and Table S1, Supporting Information). These results indicate that acetylacetonate group increases the dopant distribution in molecular scale and also photostability of emitting layer films, which can reduce efficiency roll-off in the OLEDs.[34]

To study the effects of dopant distribution on photophysical properties, we measured transient PL of low-*m* and high-*m* films with different [*D*]. In low [*D*] <15 wt%, low-*m* films showed longer PL lifetime (e.g., 1.69 µs at [*D*] = 1 wt%) than did high-*m* films (e.g., 1.364 µs at [*D*] = 1 wt%) due to aggregation of $Ir(ppy)_3$ molecules and concomitant aggregation-induced exciton quenching (i.e., TTA, TPA) in high-*m* films (Figure 4e,f). However, as [*D*] increased to 60 wt%, high-*m* films showed less decrease in PL lifetime (from 1.367 to 0.66 µs) than did low-*m* films (from 1.69 to 0.62 µs); we attributed these to electronic energy transfer from less aggregated $Ir(ppy)_3$ molecules to more aggregated adjacent ones.[35,36] To systematically analyze the dopant concentration-dependent PL lifetime, PL lifetime of low-*m* and high-*m* films with different [*D*] were fitted to modified Stern–Volmer equation (Figure 4g,h)[37]

$$\frac{\tau_0}{\tau} = 1 + k_{sv} \times [D] \tag{1}$$

where τ_0 is the PL lifetime when [*D*] = 1 wt% (lowest dopant concentration), τ is the PL lifetime with a certain [*D*], k_{sv} is a Stern–Volmer parameter. Low-*m* films were well-fitted by the Stern–Volmer equation resulting k_{sv} = 0.295 while high-*m* films cannot be well-fitted. These results indicate that

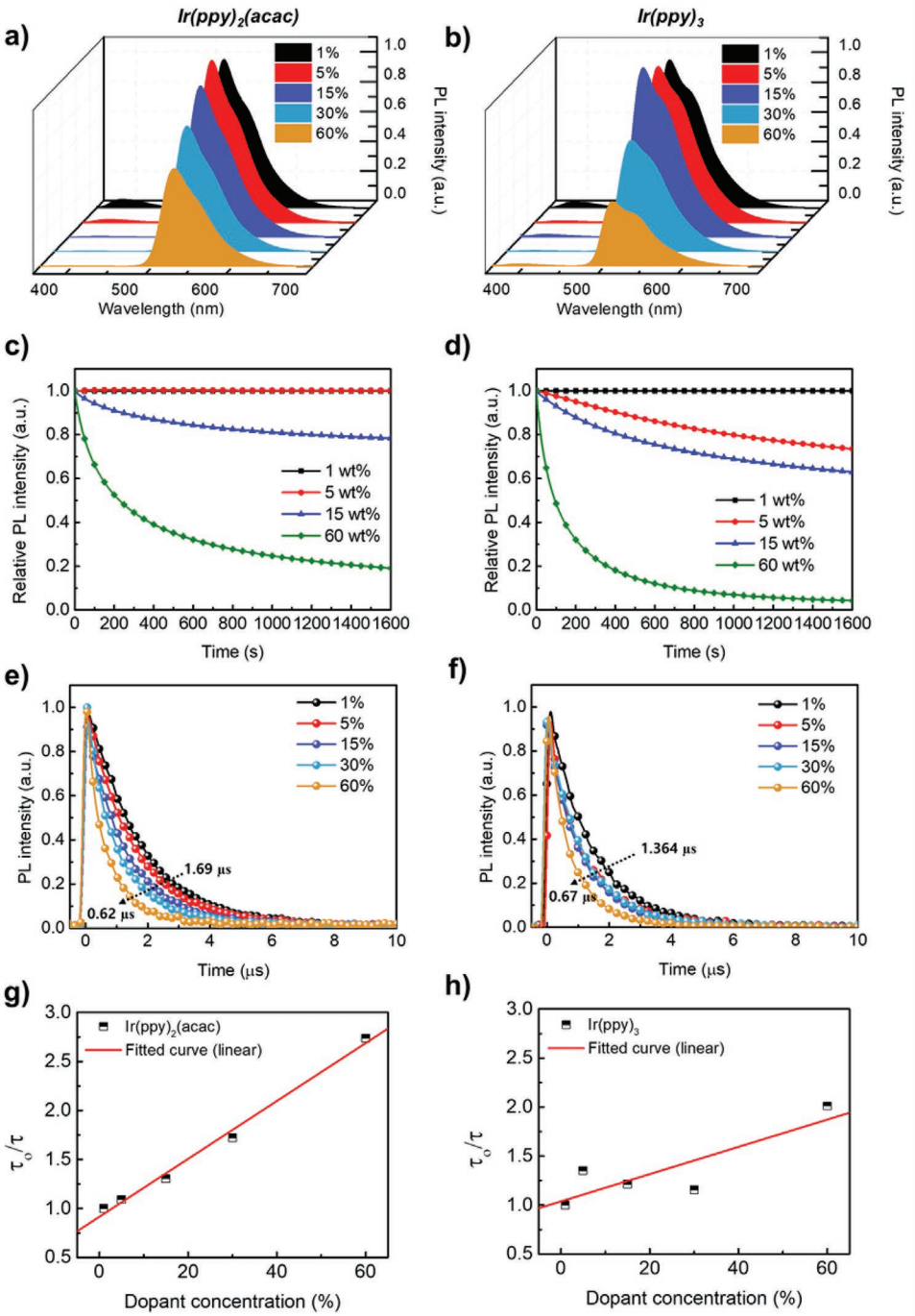

Figure 4. PL intensity of a) low-*m* ($Ir(ppy)_2(acac)$:TCTA:2PTPS) films and b) high-*m* ($Ir(ppy)_3$:TCTA:2PTPS) films with different dopant concentration. Relative PL intensity of c) low-*m* films and d) high-*m* films with different dopant concentration under the continuous light excitation. Xe lamp with $\lambda = 350$ nm is used for the excitation source. PL decay of e) low-*m* films and f) high-*m* films with different dopant concentration. Stern–Volmer plot (τ_0/τ) of g) low-*m* films and h) high-*m* films with different dopant concentration. Red line is fitted curve by Stern–Volmer equation.

$Ir(ppy)_2(acac)$ molecules in films well follow the typical intermolecular deactivation (quenching) process in which the presence of adjacent emitting dopants accelerate the decay rate of excited species (PL decay rate), while $Ir(ppy)_3$ molecules have additional factors (formation of needle-like aggregates) which affect PL decay.

To study the effects of dopants on charge transport in emitting layer, we fabricated hole-only devices (indium tin oxide (ITO)/gradient hole injection layer (GraHIL)[7]/[TCTA:2PTPS:*X*]/TCTA/MoO_3/Al) and electron-only devices (ITO/polyethylenimine-ethoxylated (PEIE)/[TCTA:2PTPS:*X*]/1,3,5-tris(*N*-phenylbenzimiazole-2-yl)benzene (TPBI)/LiF/Al), (where $X = 0$, 15% of $Ir(ppy)_3$

or $Ir(ppy)_2(acac)$) and measured their hole–current densities and electron–current densities (Figure S1, Supporting Information). Hole–current and electron–current densities were higher in devices with dopants than in devices without dopants due to direct charge injection into dopant molecules that have shallower highest occupied molecular orbital (HOMO) level (≈5.4 eV for $Ir(ppy)_3$, ≈5.6 eV for $Ir(ppy)_2(acac)$) than those of the hosts (≈5.7 eV for TCTA and ≈6.47 eV for 2PTPS).[15] Devices based on low-*m* showed higher hole–current and electron–current densities than did devices based on high-*m*. We attribute these that 1) acetylacetonate group, which reduces *m* of the phosphorescent dopants, induces uniformly distributed $Ir(ppy)_2(acac)$ molecules and suppresses the interaction between charge carriers and dopant molecules,[27–29] inducing higher charge carrier mobility in $Ir(ppy)_2(acac)$ than that in $Ir(ppy)_3$,[29,38] and 2) deeper HOMO level of $Ir(ppy)_2(acac)$ (≈5.6 eV) than that of $Ir(ppy)_3$ (HOMO ≈ 5.4 eV) facilitates efficient direct injection of holes into $Ir(ppy)_2(acac)$ from GraHIL (surface work function ≈ 5.9 eV)[7] and hopping of holes between dopants.[15]

Although we prevent dopant-aggregation and increase charge transport in the emitting layer by using phosphorescent dopant molecules with acetylacetonate group, recombination zone forms at the anode side (near the GraHIL) (Figure S2, Supporting Information) due to facilitated electron transport caused by high electron mobility of 2PTPS (≈3×10^{-4} $cm^2\ V^{-1}\cdot s^{-1}$),[15] limiting the device efficiency. To further increase the device efficiency while maintaining low efficiency roll-off, recombination zone should be formed in the center of emitting layer and broadened. We achieved these by adding a charge-balance assistant molecule, which facilitates hole transport and suppresses electron transport, into the mixed-host emitting layer. Here, we incorporated 15 wt% of a charge-balance assistant molecule, 4,4′-bis(*N*-carbazolyl)-1,1′-biphenyl (CBP), into the mixed-host emitting layer. CBP can facilitate hole transport due to higher hole mobility ($\mu_{hole} \approx 2 \times 10^{-3}$ $cm^2\ V^{-1}\cdot s^{-1}$) than that of hole-transporting host TCTA ($\mu_{hole} \approx 3 \times 10^{-4}$ $cm^2\ V^{-1}\cdot s^{-1}$),[15,29] and suppress electron hopping/transport between $Ir(ppy)_2(acac)$ molecules because CBP has similar lowest unoccupied molecular orbital (LUMO) level (≈2.8 eV) with $Ir(ppy)_2(acac)$ (LUMO level ≈3.0 eV), inducing electron trapping into CBP as well as into $Ir(ppy)_2(acac)$ (**Figure 5**a).[29,39] These can increase the charge carrier transport balance and broaden the exciton recombination zone in the center of the emitting layer (Figure 5b), which can increase the maximum device efficiency of solution-processed OLEDs.

The increased charge balance in the emitting layer by incorporation of small amount CBP can be verified by measuring hole–current densities and electron–current densities from hole-only and electron-only devices, respectively (Figure 5c), and capacitance–voltage (*C*–*V*) of solution-processed OLEDs as well (Figure 5d). OLEDs based on low-*m*:CBP showed a maximum capacitance peak at lower voltage (6.45 V) than did OLEDs based on low-*m* without CBP (maximum capacitance peak at 6.7 V), indicating facilitated charge recombination and increased charge balance.[40,41]

To evaluate our strategies in devices, we fabricated phosphorescent solution-processed OLEDs with simplified structure (ITO/GraHIL/emitting layer/TPBI/LiF/Al). Compared to the OLEDs based on high-*m*, OLEDs based on low-*m* had higher current density due to facilitated charge transport by $Ir(ppy)_2(acac)$ as discussed above (Figure 5e). Solution-processed OLEDs based on low-*m*:CBP achieved higher CE = 103.7 cd A^{-1}, power efficiency PE = 65.3 lm W^{-1} and maximum luminance $L_{EL,\,max}$ = 13 581 cd m^{-2} than did those based on high-*m* (CE = 101.5 cd A^{-1}, PE = 63.7 lm W^{-1}, $L_{EL,max}$ = 3101 cd m^{-2})[15] (Figure 5f–i). To the best of our knowledge, these are the highest CE and PE in solution-processed OLEDs to date. External quantum efficiency (EQE) of OLEDs based on low-*m*:CBP was calculated to be 26.8% by considering angular emission profile (Figure S3, Supporting Information). Solution-processed OLEDs based on high-*m*, low-*m* and low-*m*:CBP films showed similar out-coupling efficiency (Figure S3, Supporting Information) because both $Ir(ppy)_2(acac)$ and $Ir(ppy)_3$ molecules have isotropic (random) orientation in solution-processed films.[42,43] Furthermore, solution-processed OLEDs based on low-*m*:CBP showed much reduced efficiency roll-off (99.68 cd A^{-1} at L_{EL} = 100 cd m^{-2}, 76.00 cd A^{-1} at L_{EL} = 1000 cd m^{-2}) than those based on high-*m* (84.76 cd A^{-1} at L_{EL} = 100 cd m^{-2}, 23.19 cd A^{-1} at L_{EL} = 1000 cd m^{-2}) (**Table 1**; Tables S2 and S3, Supporting Information). The EL spectrum of OLEDs based on low-*m*:CBP slightly blue-shifted compared to that of OLEDs based on low-*m* (Figure S4, Supporting Information), confirming increased charge balance and shifted recombination zone from the anode side toward the center of the emitting layer.

3. Conclusion

In conclusion, we have demonstrated highly efficient solution-processed phosphorescent OLEDs with low efficiency roll-off by combining two strategies. First, we used phosphorescent dopant which has one acetylacetonate group attached to the central Iridium. Acetylacetonate group reduces dipole moment and molecular interaction energy of dopants, preventing aggregation-induced exciton quenching and increasing charge-carrier transport. We further improved the charge transport balance and facilitated charge recombination by incorporating a charge-balance assistant molecule. Ultimately, we achieved CE = 103.7 cd A^{-1} and PE = 65.3 lm W^{-1}, which are to our best knowledge the highest EL efficiencies in solution-processed OLEDs to date, and dramatically reduced efficiency roll-off in solution-processed small-molecule OLEDs even with simplified structure. We expect that our strategies will contribute to the commercialization of low-cost solution-processed OLEDs in next-generation displays and solid-state lighting.

4. Experimental Section

Fabrication and Characterization of Solution-Processed OLEDs: ITO-patterned glasses were sonicated sequentially in acetone and 2-isopropanol, each for 15 min. Dried ITO-patterned glasses were treated with UV-ozone for 15 min. Then a GraHIL (poly(3,4-ethylenedioxythiophene): polystyrene sulfonate and perfluorinated ionomer, 1:1 wt:wt) was spin-coated at 4500 rpm to give a thickness of 40 nm and baked at 150 °C for 30 min. Substrates were moved to an N_2-filled glove box, and the emitting layer, which were composed of hole transport host (TCTA), electron transport host (2PTPS), phosphorescent dopants ($Ir(ppy)_3$ or $Ir(ppy)_2(acac)$) and charge balance host (CBP) and dissolved in THF, was spin-coated to give the thickness of 40 nm. Then TPBI (50 nm), LiF

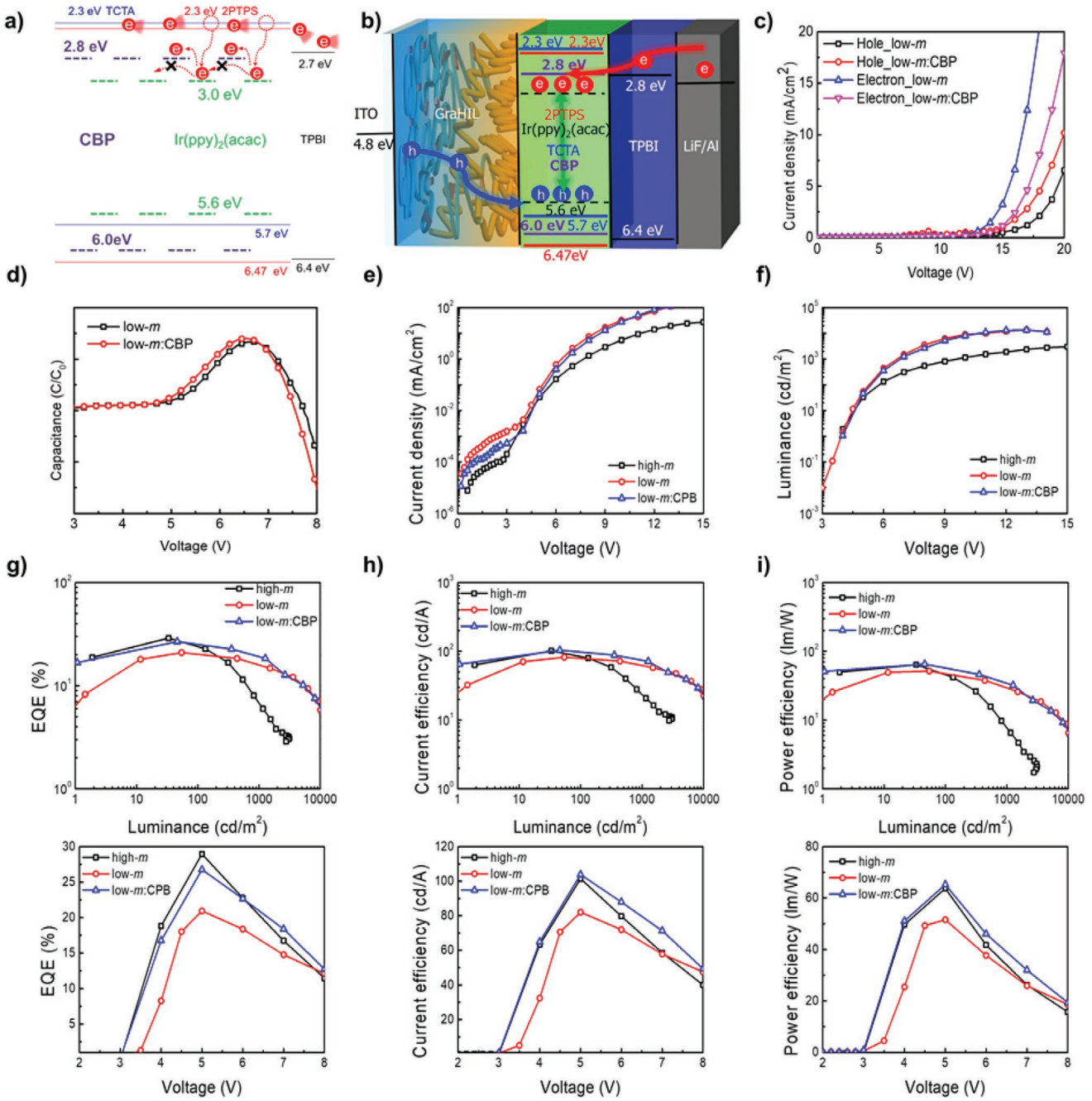

Figure 5. a) Electron transport mechanisms of low-*m* ($Ir(ppy)_2$(acac):TCTA:2PTPS):charge-balance assistant molecule (CBP) films. b) Exciton recombination mechanism in OLEDs based on low-*m*:CBP films. Schematics illustrate that CBP (charge-balance assistant molecule) traps electrons and suppresses electron transport/hopping between $Ir(ppy)_2$(acac) molecules, forming exciton recombination zone in the middle of emitting layer. c) Hole–current densities and electron–current densities measured from hole-only and electron-only devices, respectively, and d) capacitance–voltage characteristics of OLEDs based on low-*m* and low-*m*:CBP films. e) Current density–voltage, f) luminance–voltage, g) external quantum efficiency–luminance (below: linear plot of external quantum efficiency–voltage), h) current efficiency–luminance (below: linear plot of current efficiency–voltage) and i) power efficiency–luminance (below: linear plot of power efficiency–voltage) characteristics of solution-processed OLEDs based on different emitting layers (high-*m*, low-*m*, low-*m*:CBP). The device data of OLEDs based on high-*m* is taken from our previous paper for comparison.[15]

(1 nm), and Al (100 nm) were deposited sequentially in a high vacuum chamber (<10^{-7} Torr). The current–voltage–luminance characteristics of solution-processed OLEDs were measured using a Keithley 236 source measurement unit and a Minolta CS2000 spectroradiometer.

DFT Calculations: Spin-polarized DFT calculations were performed using the generalized gradient approximation with the Perdew–Burke–Ernzerhof exchange correlation functional.[44] All DFT calculations were performed using the Vienna ab initio Simulation Package.[45] Core electrons were treated with the projector augmented wave method. The cut-off energy of plane-wave expansions was set to 400 eV for all DFT calculations. The DFT-D2 method of Grimme was used to treat the van der Waals interactions.[46] For the calculation of the intermolecular

Table 1. Device efficiencies of solution-processed OLEDs based on different emitting layers.

Emitting layers	Max CE Max PE	CE, PE@ 100 cd m^{-2}	CE, PE@ 1000 cd m^{-2}
High-*m*	101.50 cd A^{-1} 63.70 lm W^{-1}	84.76 cd A^{-1} 45.90 lm W^{-1}	23.19 cd A^{-1} 7.79 lm W^{-1}
Low-*m*	82.10 cd A^{-1} 51.60 lm W^{-1}	79.40 cd A^{-1} 47.30 lm W^{-1}	61.92 cd A^{-1} 29.26 lm W^{-1}
Low-*m*:CBP	103.70 cd A^{-1} 65.30 lm W^{-1}	99.68 cd A^{-1} 57.50 lm W^{-1}	76.00 cd A^{-1} 34.36 lm W^{-1}

interactions and the single molecules, a Fermi-level smearing scheme with the width of 0.01 eV and $1 \times 1 \times 1$ gamma K-point were adopted. The convergence criteria were 1×10^{-5} eV for electronic wave functions and 3×10^{-2} eV $Å^{-1}$ for geometries.

MD Simulations: The MD simulations were performed using the GROMACS simulation package version 5.0.3.[47] The V-rescale (modified Berendsen thermostat) method was used to maintain the temperature of the system with coupling time of 0.1 ps.[48] For the pressure of the system, the Parrinello–Rahman method was adapted with coupling time of 0.2 ps.[49] The temperature and pressure were set as 300 K and 1.0 bar. The LINCS algorithm was used for the bond constraints in the system.[50] The cut-off for nonbonded interaction was 2.0 nm. The interaction parameters for the 2PTPS, TCTA, $Ir(ppy)_3$, and $Ir(ppy)_2(acac)$ molecules were generated using the SwissParam with CHARMM22 force field.[51] Each Ir atom was treated as a single point charge, as in previous MD studies.[52,53] The interaction parameters $Ir(ppy)_3$ and $Ir(ppy)_2(acac)$ were produced by parameterizing the 2-phenylpyridine (ppy) and acetylacetonato (acac) molecules. The calculations were performed in a cubic simulation box of $5.0 \times 5.0 \times 5.0$ nm with periodic boundary condition. The molecular ratio of Ir complex ($Ir(ppy)_3$ or $Ir(ppy)_2(acac)$), TCTA and 2PTPS was set as 1:1:1 with a total of 150 molecules. All molecules were solvated with THF. The energy minimization, NVT equilibrium and NPT equilibrium were performed for all systems to get stable temperature and pressure. The molecular distributions were evaluated after 20 ns simulation in NPT ensemble.

Supporting Information

Supporting Information is available from the Wiley Online Library or from the author.

Acknowledgements

Y.-H.K. and T.-H.H. contributed equally to this work. This work was supported by the National Research Foundation of Korea (NRF) grant funded by the Korea government (MSIT) (NRF-2016R1A3B1908431).

Conflict of Interest

The authors declare no conflict of interest.

Keywords

charge balance, charge-balance assistant molecules., density functional theory, dopant aggregation, molecular dynamics

Received: June 23, 2020
Revised: July 4, 2020
Published online: September 9, 2020

[1] J. Song, H. Lee, E. G. Jeong, K. C. Choi, S. Yoo, *Adv. Mater.* **2020**, *32*, 1907539.
[2] S. Reineke, F. Lindner, G. Schwartz, N. Seidler, K. Walzer, B. Lüssem, K. Leo, *Nature* **2009**, *459*, 234.
[3] M. G. Helander, Z. B. Wang, J. Qiu, M. T. Greiner, D. P. Puzzo, Z. W. Liu, Z. H. Lu, *Science* **2011**, *332*, 944.
[4] J. Kido, M. Kimura, K. Nagai, *Science* **1995**, *267*, 1332.
[5] T.-H. Han, Y. Lee, M.-R. Choi, S.-H. Woo, S.-H. Bae, B. H. Hong, J.-H. Ahn, T.-W. Lee, *Nat. Photon.* **2012**, *6*, 105.
[6] T.-W. Lee, T. Noh, H.-W. Shin, O. Kwon, J.-J. Park, B.-K. Choi, M.-S. Kim, D. W. Shin, Y.-R. Kim, *Adv. Funct. Mater.* **2009**, *19*, 1625.
[7] Y.-H. Kim, C. Wolf, H. Cho, S.-H. Jeong, T.-W. Lee, *Adv. Mater.* **2016**, *28*, 734.
[8] T.-W. Koh, J.-M. Choi, S. Lee, S. Yoo, *Adv. Mater.* **2010**, *22*, 1849.
[9] T.-W. Koh, J. A. Spechler, K. M. Lee, C. B. Arnold, B. P. Rand, *ACS Photonics* **2015**, *2*, 1366.
[10] T.-L. Wu, M.-J. Huang, C.-C. Lin, P.-Y. Huang, T.-Y. Chou, R.-W. Chen-Cheng, H.-W. Lin, R.-S. Liu, C.-H. Cheng, *Nat. Photon.* **2018**, *12*, 235.
[11] K. Tuong Ly, R.-W. Chen-Cheng, H.-W. Lin, Y.-J. Shiau, S.-H. Liu, P.-T. Chou, C.-S. Tsao, Y.-C. Huang, Y. Chi, *Nat. Photon.* **2017**, *11*, 63.
[12] B. R. Lee, E. D. Jung, J. S. Park, Y. S. Nam, S. H. Min, B.-S. Kim, K.-M. Lee, J.-R. Jeong, R. H. Friend, J.-S. Kim, S. O. Kim, M. H. Song, *Nat. Commun.* **2014**, *5*, 4840.
[13] D. Kabra, L. P. Lu, M. H. Song, H. J. Snaith, R. H. Friend, *Adv. Mater.* **2010**, *22*, 3194.
[14] E. Kim, H. Cho, K. Kim, T.-W. Koh, J. Chung, J. Lee, Y. Park, S. Yoo, *Adv. Mater.* **2015**, *27*, 1624.
[15] T.-H. Han, M.-R. Choi, C.-W. Jeon, Y.-H. Kim, S.-K. Kwon, T.-W. Lee, *Sci. Adv.* **2016**, *2*, 1601428.
[16] C. Murawski, K. Leo, M. C. Gather, *Adv. Mater.* **2013**, *25*, 6801.
[17] J. Lim, Y. S. Park, K. Wu, H. J. Yun, V. I. Klimov, *Nano Lett.* **2018**, *18*, 6645.
[18] M. A. Baldo, C. Adachi, S. R. Forrest, *Phys. Rev. B* **2000**, *62*, 10967.
[19] H. Zamani Siboni, H. Aziz, *Appl. Phys. Lett.* **2012**, *101*, 063502.
[20] G. G. Malliaras, J. R. Salem, P. J. Brock, J. C. Scott, *J. Appl. Phys.* **1998**, *84*, 1583.
[21] N. C. Giebink, S. R. Forrest, *Phys. Rev. B* **2008**, *77*, 235215.
[22] J. Kalinowski, W. Stampor, J. Szmytkowski, D. Virgili, M. Cocchi, V. Fattori, C. Sabatini, *Phys. Rev. B* **2006**, *74*, 085316.
[23] Y. Luo, H. Aziz, Z. D. Popovic, G. Xu, *Appl. Phys. Lett.* **2006**, *89*, 103515.
[24] Y. Li, G. Xie, S. Gong, K. Wu, C. Yang, *Chem. Sci.* **2016**, *7*, 5441.
[25] Y. J. Cho, K. S. Yook, J. Y. Lee, *Adv. Mater.* **2014**, *26*, 6642.
[26] N. Aizawa, Y. J. Pu, M. Watanabe, T. Chiba, K. Ideta, N. Toyota, M. Igarashi, Y. Suzuri, H. Sasabe, J. Kido, *Nat. Commun.* **2014**, *5*, 5756.
[27] S. Reineke, T. C. Rosenow, B. Lüssem, K. Leo, *Adv. Mater.* **2010**, *22*, 3189.
[28] A. Graf, P. Liehm, C. Murawski, S. Hofmann, K. Leo, M. C. Gather, *J. Mater. Chem. C* **2014**, *2*, 10298.
[29] N. Matsusue, Y. Suzuki, H. Naito, *Jpn. J. Appl. Phys.* **2005**, *44*, 3691.
[30] F.-C. Chen, S.-C. Chang, G. He, S. Pyo, Y. Yang, M. Kurotaki, J. Kido, *J. Polym. Sci., Part B: Polym. Phys.* **2003**, *41*, 2681.
[31] S. Takayasu, T. Suzuki, K. Shinozaki, *J. Phys. Chem. B* **2013**, *117*, 9449.
[32] H. Wang, Q. Liao, H. Fu, Y. Zeng, Z. Jiang, J. Ma, J. Yao, *J. Mater. Chem.* **2009**, *19*, 89.
[33] Y. T. Kim, J. B. Seol, Y. H. Kim, H. J. Ahn, C. G. Park, *Small* **2017**, *13*, 1602874.
[34] J. R. Gong, L. J. Wan, S. Bin Lei, C. L. Bai, X. H. Zhang, S. T. Lee, *J. Phys. Chem. B* **2005**, *109*, 1675.
[35] C. R. Kagan, C. B. Murray, M. Nirmal, M. G. Bawendi, *Phys. Rev. Lett.* **1996**, *76*, 1517.
[36] N. Kholmicheva, P. Moroz, H. Eckard, G. Jensen, M. Zamkov, *ACS Energy Lett.* **2017**, *2*, 154.

[37] X. Wu, W. Wu, X. Cui, J. Zhao, M. Wu, *J. Mater. Chem. C* **2016**, *4*, 2843.
[38] T. Tsuzuki, S. Tokito, *Adv. Mater.* **2007**, *19*, 276.
[39] N. Matsusue, S. Ikame, Y. Suzuki, H. Naito, *Appl. Phys. Lett.* **2004**, *85*, 4046.
[40] T.-H. Han, Y.-H. Kim, M. H. Kim, W. Song, T.-W. Lee, *ACS Appl. Mater. Interfaces* **2016**, *8*, 6152.
[41] T.-H. Han, W. Song, T.-W. Lee, *ACS Appl. Mater. Interfaces* **2015**, *7*, 3117.
[42] C.-K. Moon, K.-H. Kim, J. W. Lee, J.-J. Kim, *Chem. Mater.* **2015**, *27*, 2767.
[43] T. Lampe, T. D. Schmidt, M. J. Jurow, P. I. Djurovich, M. E. Thompson, W. Brütting, *Chem. Mater.* **2016**, *28*, 712.
[44] J. P. Perdew, K. Burke, M. Ernzerhof, *Phys. Rev. Lett.* **1996**, *77*, 3865.
[45] G. Kresse, J. Furthmüller, *Phys. Rev. B* **1996**, *54*, 11169.
[46] S. Grimme, *J. Comput. Chem.* **2006**, *27*, 1787.
[47] B. Hess, C. Kutzner, D. Van Der Spoel, E. Lindahl, *J. Chem. Theory Comput.* **2008**, *4*, 435.
[48] G. Bussi, D. Donadio, M. Parrinello, *J. Chem. Phys.* **2007**, *126*, 014101.
[49] M. Parrinello, A. Rahman, *J. Appl. Phys.* **1981**, *52*, 7182.
[50] B. Hess, H. Bekker, H. J. C. Berendsen, J. G. E. M. Fraaije, *J. Comput. Chem.* **1997**, *18*, 1463.
[51] V. Zoete, M. A. Cuendet, A. Grosdidier, O. Michielin, *J. Comput. Chem.* **2011**, *32*, 2359.
[52] C. Tonnelé, M. Stroet, B. Caron, A. J. Clulow, R. C. R. Nagiri, A. K. Malde, P. L. Burn, I. R. Gentle, A. E. Mark, B. J. Powell, *Angew. Chem., Int. Ed.* **2017**, *56*, 8402.
[53] T. Lee, B. Caron, M. Stroet, D. M. Huang, P. L. Burn, A. E. Mark, *Nano Lett.* **2017**, *17*, 6464.